Constrained guidance for spacecraft proximity operations under electrostatic perturbations

Kieran Wilson
Graduate Research Assistant
Aerospace Engineering Sciences
University of Colorado Boulder
Boulder, Colorado 80303
kieran.wilson@colorado.edu

Hanspeter Schaub
Glenn L. Murphy Endowed Chair
Aerospace Engineering Sciences
University of Colorado Boulder
Boulder, Colorado 80303

Abstract— **Electrostatic perturbations can have significant effects during proximity operations in high earth orbits, with torques achieving levels over 5 mN-m during severe charging events. These torques can impart significant rotational rates to uncontrolled bodies, such as debris or servicing clients, during rendezvous and proximity operations. A sub optimal, but deterministic and computationally efficient, sampling-based method to minimize the impact of these torques during rendezvous is presented here, combining prior innovations in rapidly computing the electrostatic torque between bodies and in determining the electrostatic potential on objects remotely. This method is applied to a simulated servicing scenario, and found to reduce the accumulated rotational rates of the target by over 50%, yielding significant improvements in control effort, and potential improvements in safety. The method can also be applied to position the servicer to impart a desired torque on the target, allowing it to counteract the effects of SRP or potentially reduce the rotational rate of a debris object prior to grappling.**

TABLE OF CONTENTS

1. INTRODUCTION

Recent work has demonstrated the potential impact of electrostatic perturbations on proximity operations, particularly in high earth and geostationary orbital regimes where high spacecraft potentials may be encountered [1]. Spacecraft in the GEO region, for instance, can charge to 10s of kilovolts depending on local space weather conditions [2]. While such charging events are relatively infrequent, proximity operations during these times are significantly perturbed by the electrostatic forces and torques acting between the spacecraft; cases with an uncontrolled target body, such as a servicing or debris remediation mission, are particularly affected. With the increasing popularity and necessity of such missions in high earth orbits, there is a need to consider these induced dynamical effects which can impart target tumble rates exceeding a degree per second to an uncontrolled target during rendezvous [1]. Such rotational rates significantly complicate rendezvous, imposing high propellant usage demands on the servicer and posing a much more challenging navigation scenario than rendezvous with a non-rotating target body.

The system dynamics between two charged spacecraft are highly nonlinear, with mutual forces and torques dependent on the positions and attitudes of both spacecraft, as well as their geometries (which dictate charge distributions) and electrostatic potentials. Two innovations make rapid guidance and control in these scenarios possible: the development of methods to accurately and remotely determine the potential on a co-orbiting object, and a method for rapidly evaluating the electrostatic forces and torques between nearby bodies. The electrostatic potential sensing method is based on observations of x-ray and electron spectra excited during energetic electron bombardment of the target, either in a controlled manner using an electron gun mounted to the servicer, or by relying on hot electrons present in the ambient plasma environment [3]. Force and torque computations can then be performed using the multi-sphere method (MSM), a computationally efficient means of approximating the electric fields around a body to within a few percent, given knowledge of the target's geometry and electrostatic potential [4].

The goal of this work is to combine these innovations in a guidance and control framework to meet proximity operation goals while minimizing the impact of electrostatic perturbations, either in positional errors, fuel consumption, or tumble rates imparted to the target. These electrostatic perturbations are unique and different compared to electromagnetic interactions which can arise in cases with alternating currents. Combining touchless potential sensing and MSM will allow for rapid evaluation of the anticipated forces and torques, suitable for implementation aboard flight hardware. This work will enable safer, more robust proximity operations during periods of heightened electrostatic charging, which in turn could enable expanded opportunities for engaging in proximity operations.

This paper is organized as follows. First, the system dynamics will be established, consisting of translational and rotational dynamics. The perturbing forces and torques created by electrostatic interactions will be introduced, along with methods for rapidly evaluating the force and torque contributions, and the relative magnitudes of each compared to those exerted by solar radiation pressure.

A guidance strategy will then be introduced which enables rapid computation of a torque-minimal approach to an inert target object. This strategy will be numerically simulated, and performance compared to an approach that does not account for electrostatic perturbations.

978-1-7281-7436-5/21/$31.00

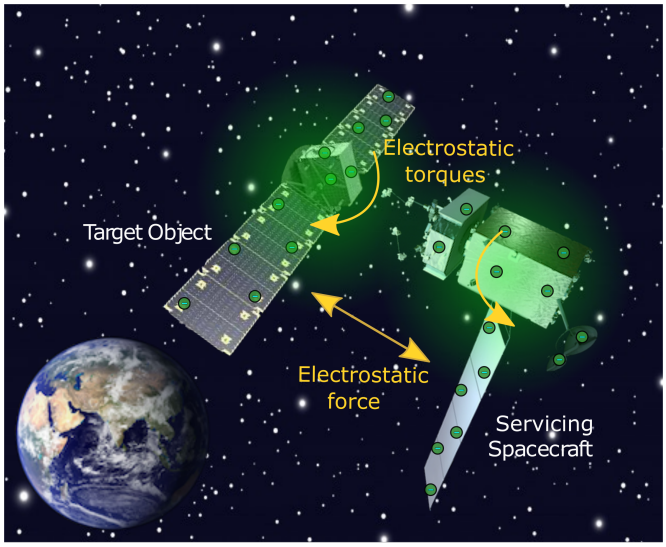

Figure 1. Illustration of electrostatic interactions between a servicer and a client spacecraft.

2. Problem Scenario

The scenario relevant to this work involves a servicer approaching an inert target spacecraft, where both spacecraft have accumulated significant electrostatic potentials as a result of interactions with the space environment. While significant (>kV level) charging events at geostationary orbit are relatively rare, occurring perhaps a few days per year on average, they can occur more frequently during periods of heightened solar activity [5]. Additionally, some components of spacecraft and debris objects may not be continuously conducing with the spacecraft frame, and may be composed of dielectric or other materials which experience charging differently than conducting metal structures. These components may be subject to significantly higher levels of charging than a fully conducting spacecraft structure, with data from the ATS-6 mission showing a Kapton element at a floating potential having over 100x the electrostatic potential of the conducting spacecraft frame [6].

Additionally, other work has shown that the use of spacecraft charging models to estimate the electrostatic potential on an object based on space weather conditions can dramatically mis-estimate the true potential of the spacecraft, so it is important not to simply assume a potential on a target body, but actively monitor the potential during proximity operations [7], [8].

3. Dynamics

The analysis here covers a two-craft rendezvous scenario in a geostationary graveyard orbit. It includes electrostatic perturbations, and includes comparisons with the other dominant perturbation in the GEO regime, solar radiation pressure (SRP). The orbital regimes which are most susceptible to prolonged, high intensity electrostatic charging tend to have negligible drag, so such considerations are omitted [9]. Additionally, plume impingement is not considered here, as it is highly dependent on thruster orientations and placement, and as such can be either largely mitigated or magnified depending on specific operational parameters.

Relative motion dynamics

The fundamental scenario of interest is of one spacecraft actively approaching an inert target body. Non-Keplerian forces (SRP and electrostatics) act on both spacecraft, so both are established as deputies relative to a virtual Keplerian Chief, which is used as the origin of the Hill frame. The target spacecraft is initialized at the origin. Because the translational dynamics of the problem under investigation here involves small separation distances, short time scales relative to the orbital period and a large orbital radius with small eccentricity, the relative motion dynamics are well captured by the Hill-Clohessy Wiltshire equations of linearized relative motion, as given in Equation 1 [10]. The n terms refer to the orbital mean motion, while a_x, a_y, a_z refer to perturbing acceleration components in the Hill frame, whether from SRP, electrostatics, or thruster actuation.

$$\begin{aligned} \ddot{x} &= 3n^2 x + 2n\dot{y} + a_x \\ \ddot{y} &= -2n\dot{x} + a_y \\ \ddot{z} &= -n^2 z + a_z \end{aligned} \tag{1}$$

Rotational dynamics

Rotational dynamics are described by Euler's equation for rigid bodies, given by Reference [11] as

$$[I]\dot{\boldsymbol{\omega}} = -[\tilde{\boldsymbol{\omega}}][I]\boldsymbol{\omega} + \boldsymbol{L} \tag{2}$$

where the tilde operator represents the skew symmetric matrix of a vector, given for a three element vector as

$$[\tilde{\boldsymbol{\omega}}] = \begin{bmatrix} 0 & -\omega_3 & \omega_2 \\ \omega_3 & 0 & -\omega_1 \\ -\omega_2 & \omega_1 & 0 \end{bmatrix}. \tag{3}$$

Accurately computing the rotational motion of the servicer and target therefore requires knowledge of the mass properties for both, primarily the inertia matrix $[I]$ and the center of mass location. Publicly available masses and dimensional information for different spacecraft were used to generate CAD models, which could be used to estimate the center of mass and inertia matrices for each. Such methods provide a reasonable set of mass properties for simulations. Rigid bodies were assumed for both structures.

Spacecraft attitudes were propagated using quaternions, with the quaternion kinematic equations given by Reference [11] as

$$\dot{\boldsymbol{\beta}} = \frac{1}{2}\begin{bmatrix} \beta_0 & -\beta_1 & -\beta_2 & -\beta_3 \\ \beta_1 & \beta_0 & -\beta_3 & \beta_2 \\ \beta_2 & \beta_3 & \beta_0 & -\beta_1 \\ \beta_3 & -\beta_2 & \beta_1 & \beta_0 \end{bmatrix}\begin{bmatrix} 0 \\ \omega_1 \\ \omega_2 \\ \omega_3 \end{bmatrix}. \tag{4}$$

Therefore, at each timestep the perturbing torques and current rotational rates can be used to update the attitude states for both spacecraft.

Other Perturbations

Given the relatively high electrostatic potentials of interest in this problem, it is worth considering the dynamic effects of charged spacecraft interactions with the environment. Two interactions are considered: the effect of the charged spacecraft's interactions with Earth's magnetic field (Lorentz force)

and ionospheric drag, due to the interaction of a charged spacecraft with ambient charged particles. The total charge on a spacecraft charged to a near-record -20 kV is approximately 1×10^{-5}C. The Lorentz force can then be computed as

$$\boldsymbol{F} = q(\boldsymbol{E} + \boldsymbol{v} \times \boldsymbol{B}) \tag{5}$$

which, given a nominal GEO magnetic field intensity of 106 nT [12], orbital velocity $v = 3$ km/s and electric field intensity on the order of 1 mV/m [13], the Lorentz force can be estimated to be on the order of 10^{-8} N - approximately ⅓ the gravitational force exerted by the moon, and approximately 5-6 orders of magnitude smaller than inter-craft electrostatic forces.

Likewise, plasma densities at GEO are often very low compared to LEO orbits, with typical plasma densities on the order of 10^5 ions per cubic meter [] compared to some 5 orders of magnitude greater in LEO (typically 5×10^{10} per cubic meter at 500 km). These low plasma densities, combined with lower orbital velocities than in LEO, result in negligible ionospheric drag forces.

While the contributions of Lorentz forces and ionospheric drag are negligible, the dominant perturbation at high earth orbits is typically SRP [14], which can affect a spacecraft's inertial acceleration and also impart significant torques. The first order SRP model used here divides each spacecraft into a series of rectangular elements, representing a face of a solar array or a side of a bus for example.

$$\boldsymbol{F}_i = -P_{\text{SRP}} \left((1 - \beta_{s,i})\hat{\boldsymbol{s}} + 2 \left(\beta_{s,i} \cos(\theta_i) + \frac{1}{3}\beta_{D,i} \right) \hat{\boldsymbol{n}}_i \right) \cdot \cos(\theta_i) A_i \tag{6}$$

where β_s represents the specular reflection coefficient, and β_D is the diffuse reflection coefficient for the given element. The sun direction unit vector is given by $\hat{\boldsymbol{s}}$, while $\hat{\boldsymbol{n}}_i$ is the face normal unit vector; θ_i describes the angle between $\hat{\boldsymbol{s}}$ and $\hat{\boldsymbol{n}}_i$. A_i is the area of the given element. Reflection and absorption coefficients for representative material surfaces were taken from Reference [15].

Electrostatic force and torque computation

Traditional methods for computing the electrostatic forces and torques between bodies rely on finite element methods. These techniques are typically highly accurate, but require significant computational resources which make them impractical for modeling system dynamics.

However, the recently developed Multi-Sphere Method (MSM) can rapidly evaluate the electrostatic interactions between bodies to within a few percent accuracy, and at a fraction of the computational cost [16], [4]. This method discretizes an object as a series of spheres, with the sphere positions and radii tuned to match a parameter of the object (typically the object's self-capacitance). A straightforward method to choose sphere radii is to match the capacitance of the sphere to a corresponding finite element; the sphere can then be located at the element centroid in the heterogeneous surface MSM development [4]. Analytic expressions for the mutual capacitance effects of multiple spheres can then be used to determine the charge on each sphere for a given voltage. The simplest example is the case of two nearby

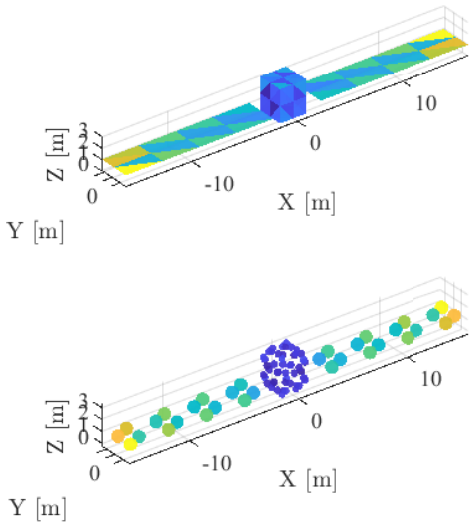

Figure 2. Example of a spacecraft model discretized into 84 elements for use in the Method of Moments finite element formulation, and the equivalent Multi-Sphere Model.

spheres, which can be represented as

$$\begin{bmatrix} q_1 \\ q_2 \end{bmatrix} = \underbrace{\frac{r}{k_c\left(r^2 - R_1R_2\right)} \begin{bmatrix} rR_1 & -R_1R_2 \\ -R_1R_2 & rR_2 \end{bmatrix}}_{C_V} \begin{bmatrix} V_1 \\ V_2 \end{bmatrix}. \tag{7}$$

where R_1, R_2 are the sphere radii, and r represents the L2 norm distance between the spheres. This can be expanded to an $n \times m$ matrix, where the first object is composed of n spheres and the second of m spheres, as seen in Equation 8.

$$\begin{pmatrix} V_1 \\ V_2 \\ \vdots \\ V_n \end{pmatrix} = k_c \begin{bmatrix} 1/R_1 & 1/r_{1,2} & \dots & 1/r_{1,n} \\ 1/r_{2,1} & 1/R_2 & \dots & 2/r_{2,n} \\ \vdots & \vdots & \ddots & \vdots \\ 1/r_{n,1} & 1/r_{n,2} & \dots & 1/R_n \end{bmatrix} \begin{pmatrix} Q_1 \\ Q_2 \\ \vdots \\ Q_n \end{pmatrix} \tag{8}$$

This can be expressed as the simple relation relating the charge and potential

$$\mathbf{V} = [\mathbf{S}]\mathbf{Q} \tag{9}$$

where $[S]$ is the elastance matrix, which is the inverse of the capacitance matrix. Therefore, if the voltages, positions and radii of each sphere are known, then the charge on each can be computed by inverting Equation 9.

Once the charge on each sphere is known, then the forces and torques between each body can be evaluated. The force contributions of each charge in body 2 (q_j) acting on each charge in body 1 ((q_i) can be evaluated as

$$\boldsymbol{F} = k_c \sum_{j=1}^{n_1} q_j \left(\sum_{i=1}^{n_2} \frac{q_i}{r_{i,k}^3} \boldsymbol{r}_{i,j} \right) \tag{10}$$

This can be extended to determine the resultant torque as

$$\boldsymbol{L}_O = k_c \sum_{j=1}^{n_1} q_j \left(\sum_{i=1}^{n_2} \frac{q_i}{r_{i,j}^3} \boldsymbol{r}_i \times \boldsymbol{r}_{i,j} \right) \tag{11}$$

It is important to note that r_i is the distance from a sphere in the body of interest to the center of mass of that body, while $r_{i,j}$ represents the distance from sphere i in body 1 to sphere j in body 2.

While computationally efficient, the MSM formulation still requires initialization using a finite element model, which provides a truth capacitance used to tune each sphere position and radius to accurately capture the charge distribution across the surface. The method of moments (MOM) is used here, as seen in Figure 2 and described in detail by Reference [4]. For comparison, a high fidelity MoM finite element setup required approximately 1000 seconds of computation time to find the forces and torques acting between two spacecraft composed of 500 elements each. The equivalent fidelity MSM model required less than 0.2 seconds, for a 10^4 speed up; lower fidelity models can be evaluated much faster still with minimal loss of accuracy [4]. The finite element truth model only needs to be computed once for a structure, and the resulting multisphere model is then valid for any future case, including with flexible or time-varying structures, or multiple spacecraft operating in close proximity [17]. This makes MSM ideally suited for faster-than-realtime dynamics propagation, or real-time guidance.

Rigid bodies are assumed for the MSM structures here. However, the MSM formulation can be readily applied to time-varying geometries, such as servicer solar arrays rotating to track the sun or extending robotic arms [17]. These time-varying structures can be solved without requiring an update of the computationally-intensive finite element computation step, but can instead be updated using only the MSM formulation.

Sensing electrostatic potentials remotely

In order to effectively utilize the MSM to quickly and accurately compute electrostatic forces and torques, the electrostatic potential of each object must be known.

Several flight-proven techniques exist to determine the electrostatic potential of a spacecraft equipped with requisite instruments, as a servicer would be assumed to carry. These typically rely on measurements of some parameter of the plasma environment to determine the spacecraft potential relative to the plasma; as space plasmas are typically regarded as neutral, this provides an absolute estimate of the quantity of excess charge on an object [18].

While methods to assess the potential of an instrumented spacecraft relative to the surrounding plasma have been well established for decades, only recently have two methods been developed to determine the electrostatic potential of an un-instrumented object without requiring physical contact. Reference [19] describes a technique to estimate the potential of a target to within $\sim$ 100 volts using bremsstrahlung x-rays emitted by the interactions of energetic electrons with the target. The energetic electrons could either come from an electron gun on the servicer, or the ambient plasma in high earth orbit [20]. The second method is covered in Reference [21], and involves measuring the electrons emitted from the target through either solar-induced photoemission, or secondary electrons generated by incident energetic electrons in the ambient plasma or from an electron beam. The electron-based method can resolve target potentials with an accuracy of $\sim$ 10 volts. However, the electron-based method has far lower observability of the target potential, with a useful signal available for only $\sim$ 10% of servicer-target orientation combinations for a sample spacecraft shape tested. By contrast, the bremsstrahlung-based method showed signal availability in over 70% of servicer-target test orientations [3].

These two methods can be used in tandem to provide an accurate estimate of the target's electrostatic potential, with the bremsstrahlung-based method enabling a a relatively low-resolution estimate with high levels of observability, while the electron-based method will enable high-resolution measurements with low availability. An adaptive Kalman filter is used in Reference [3] to fuse the measurements of each method into a single estimate of the relative potential between the spacecraft.

A relevant concern is whether such accuracy is sufficient for effective modeling of inter-craft forces and torques. A first order sensitivity analysis is introduced here to evaluate the required potential sensing accuracy, as well as sensitivity of the computed forces and torques to ranging and attitude estimation.

Sensitivity to estimated potential and range

A few fundamental assumptions underpin the use of MSM here. First, the sphere radii and positions are derived from a finite element model of each spacecraft, taken as a ground truth. This truth model requires accurate models of the surface geometry of both spacecraft must be known; through a combination of a priori knowledge of the target and systems like LiDAR, this is readily achievable [22].

Next, the relative position and attitude of the spacecraft must be known to accurately compute the relative positions of each pair of spheres. Relative pose estimation remains an area of active research, but it is possible to obtain pose estimates of an uncooperative target with less than a degree of error using modern 3D flash LiDARs, stereo cameras or other techniques [23].

Torque is computed as the cross product between the electrostatic force vector and the radius between the point where the force is applied to the body and the body's center of mass. The force vector is a product of the electrostatic interactions, and derived from the MSM. However, the torque computation then requires an accurate evaluation of the target body's center of mass. Furthermore, to predict the resultant rotational dynamics requires an accurate estimate of the target's inertia matrix. For a cooperative servicing target these values may be well documented, even in an end of life scenario. However, for a debris object these parameters may require estimation on-orbit by observing the rotational properties of the target. If the shape and potential of the target (either as a result of natural charging or the use of an electron beam to actively induce potentials) are known it may be possible to use electrostatic interactions and proximity flight to deliberately introduce perturbing torques to the target, and the target's resulting rotational behavior then used to estimate its inertia parameters. The ability to apply a known external torque to a body may enable improvements in performance over previously proposed methods to estimate the inertia properties of tumbling bodies like those described by Reference [24].

Finally, the electrostatic potential of both the servicer and

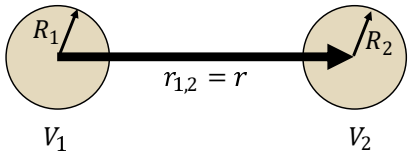

Figure 3. Illustration of two-sphere system evaluated.

target must be known. The methods described in References [19] and [21] can achieve consistent target voltage estimates within 100V or less. However, no work has yet been conducted to evaluate the potential estimation accuracy required for sufficiently accurate dynamic evaluations. In related work, Reference [25] explores the impact of erroneous total system charge product (the product of multiplying the charges on each spacecraft) on the closed-loop control stability characteristics of an actively charged Electrostatic Tractor debris tugging scenario.

While the electrostatic potential may be sensed remotely by the methods in References [19] and [21], electrostatic charges are responsible for producing force and torque interactions between the bodies. The charge is related to the potential on a body by the body's capacitance, which is chiefly determined by the body's surface geometry.

A reduced-order analysis is developed to evaluate the sensitivity of the computed force and torque to the estimated electrostatic potential, and intercraft distance. To gain analytic insight into the sensitivity, each body is modeled as a single sphere, as seen in Figure 3, the simplest configuration which still enables the capture of mutual capacitance effects. The force acting between the spheres can then be found as

$$F = \frac{k_c q_1 q_2}{r^2}. \tag{12}$$

Therefore, electrostatic charges on each sphere must be calculated as a function of their potentials, which can be found as in Equation 8, repeated here for convenience:

$$\begin{bmatrix} q_1 \\ q_2 \end{bmatrix} = \frac{r}{k_c\,(r^2 - R_1R_2)} \begin{bmatrix} rR_1 & -R_1R_2 \\ -R_1R_2 & rR_2 \end{bmatrix} \begin{bmatrix} V_1 \\ V_2 \end{bmatrix}. \tag{13}$$

The upper right and lower left elements of the capacitance matrix represent mutual capacitance effects, caused by the interactions of the two bodies. These are expanded as

$$q_1 = \frac{r}{k_c\,(r^2 - R_1R_2)}(rR_1V_1 - R_1R_2V_2) \tag{14}$$

$$q_2 = \frac{r}{k_c\,(r^2 - R_1R_2)}(rR_2V_2 - R_1R_2V_1) \tag{15}$$

Combining this expansion with Equation 12 yields a force expression as

$$F = \left(\frac{r}{k_c\,(r^2 - R_1R_2)}\right)^2 \big((r^2 + R_1R_2)V_1V_2 - rR_1V_2^2 - rR_2V_2^2\big). \tag{16}$$

where the leading term is constant with respect to voltage.

However, in practice, V_2 will represent the measured *relative* potential between sphere 1 and 2, as it is based on a measurement system being aboard sphere 1. Therefore, the true *absolute* potential of sphere two relative to the common ground for the two bodies (the ambient plasma) is the sum of the errors in the servicer's measurement of its own potential relative to the plasma, and also the error in the servicer's measurement of the target's potential relative to itself. Therefore, the force between the bodies becomes

$$F = \left(\frac{r}{k_c\,(r^2 - R_1R_2)}\right)^2 \big((r^2 + R_1R_2)V_1(V_1+V_2) - rR_1(V_1+V_2)^2 - rR_2(V_1+V_2)^2\big). \tag{17}$$

Typically, the effects of electrostatic interactions only become significant for cases where charging exceeds a few kV. While the sensitivity analysis provides a relative sensitivity, the methods used to remotely measure electrostatic potentials tend to be better characterized by an absolute uncertainty rather than a percentage. However, the typical 1σ uncertainty in the measurements are in the range of 10-100 V, so for a worst-case scenario with a minimum relevant charge level of 1000V with 300V uncertainty (a 3σ level) would result in a 30% relative potential uncertainty.

A common method for measuring the potential of a spacecraft relative to the ambient plasma is to use an ion energy spectrometer to determine the evolution of a stable reference line in the background plasma ion population. If a given proton population is known to have an energy of, for instance, 5 eV, then the observed energy of that population provides a measure of negative charging relative to the plasma. Similar methods can be used with electron populations to measure positive potentials. These methods are limited in accuracy by the energy resolution of the instrument used, but can typically resolve spacecraft potentials to within a few percent ($< 5\%$) [18].

The sensitivity of force to error in either V_1 (the voltage of the servicer) or V_2 (the potential of the target relative to the servicer) can be evaluated by taking the ratio of the partial derivatives of the electrostatic force with respect to V_1 and V_2. The resultant ratio, seen in Equation 18, is a function of not just V_1, V_2 but also of the problem geometry.

The ratio of $\partial F/\partial V_1 \big/ \partial F/\partial V_2$ is independent of the base voltage of each sphere (the ratio remains the same regardless of V_1, V_2 as long as $V_1 = V_2$).

$$\frac{\partial F/\partial V_1}{\partial F/\partial V_2} = \frac{(2V_1+V_2)(r^2 + R_1R_2) - 2R_1V_1r - 2R_2r(V_1+V_2)}{V_1(r^2 + R_1R_2) - 2R_2r(V_1+V_2)} \tag{18}$$

Ultimately, the system, as expected, is far more sensitive to V_1 than V_2. The exact value of the sensitivity ratio is a function of both voltages and the positions of each sphere, but is typically somewhere between 3 and 10 for most reasonable combinations of potentials and positions. It is assumed that the potentials on both spacecraft should be similar, as they are exposed to similar space environment conditions, but differences in construction and material properties may result in significant (kV level) differences. For a nominal case where each spacecraft is charged to 10 kV at 10 meter

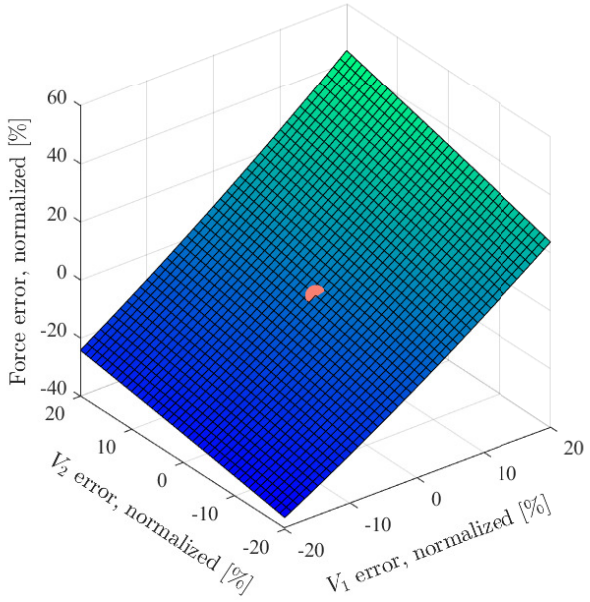

Figure 4. Force error as a result of errors in V_1 and V_2. Orange point represents the origin, for reference.

separation, Figure 4 illustrates the relationship between misestimated potentials on each sphere and the resultant force. As expected, the force error is significantly more affected by errors in V_1 than V_2, with the relation nearly linear in this range. Nonlinearities in this relation become more pronounced as errors exceed 20%, but it is reasonable that this figure should account for most potential measurement uncertainties using existing techniques.

4. CONTROL

The system dynamics are inherently nonlinear, due to the coupling of position, attitude and resultant force and torque. Therefore, a nonlinear Lyapunov-derived Cartesian feedback controller was developed to track the desired reference trajectory computed by the guidance system, as [11]

$$\boldsymbol{u} = -\ddot{\boldsymbol{\rho}} - [K_1]\,\Delta\boldsymbol{r} - [K_2]\,\Delta\dot{\boldsymbol{r}}. \tag{19}$$

Here the term $\ddot{\boldsymbol{\rho}}$ represents the relative inertial acceleration between the reference point in the $\mathcal{T}$ frame and the $\mathcal{H}$ frame as a result of differential gravitational accelerations and the rotation of the target body with respect to the $\mathcal{H}$ frame. It is assumed that the target body's rotational rates and pose are known, likely through a combination of image-based and LiDAR-based methods. By feeding forward on these known relative accelerations, the servicer achieves better tracking at lower control effort cost.

As the target body rotates, the reference position will accelerate relative to the Hill frame. This acceleration is computed as

$$\begin{aligned}\ddot{\boldsymbol{r}}_{T/S} = \boldsymbol{r}''_{T/S} + \dot{\boldsymbol{\omega}}_{T/H} \times \boldsymbol{r} + 2\boldsymbol{\omega} \times \boldsymbol{r}' \\ + \boldsymbol{\omega}_{T/H} \times \left(\boldsymbol{\omega}_{T/H} \times \boldsymbol{r}\right)\end{aligned} \tag{20}$$

where the prime right superscript denotes a body-frame derivative, and dots a Hill-frame derivative.

The terms for $\dot{\boldsymbol{\omega}}$ are computed from Equation 2, rearranging as

$$\dot{\boldsymbol{\omega}} = -[I]^{-1}[\tilde{\boldsymbol{\omega}}][I]\boldsymbol{\omega} + [I]^{-1}\boldsymbol{L} \tag{21}$$

where the principal components of $[I]$ are on the order of 10000 kg-m^2 for a large, fully deployed geostationary satellite, and the electrostatic torques are on the order of 1 mN-m. With rotational rates of $\sim$ 0.002 rad/s in a given axis (0.1 deg/s), $\dot{\boldsymbol{\omega}}$ can be expected to be on the order of 10^{-5} rad/s^2. These are small compared to the other terms in the acceleration equation, and could be dropped if there is significant uncertainty in the modeling of the target inertia matrix or torques acting on the target body.

The attitude of the servicer must follow a time-varying reference to maintain a line of sight vector between the servicer's relative navigation sensors and the docking point on the target. The goal of the attitude controller is therefore to track the target's rotation such that the navigation system is always aligned to the docking port.

The attitude controller acts independently of the translation controller, and like the translation controller, has a maximum control effector limit but no minimum. This correlates well to an attitude control system reliant on momentum exchange devices like reaction wheels or control moment gyroscopes, while a reaction control system or other thruster-based method is used to apply translational control. The torque control limit is set to 100 mN-m, approximately the torque available from large reaction wheels like the Honeywell HR-12 series [26].

The attitude controller feeds back on the spacecraft attitude MRP, and is given by Reference [11] as

$$\boldsymbol{u} = -K\boldsymbol{\sigma} - P\delta\boldsymbol{\omega} + [I](\dot{\boldsymbol{\omega}}_r - [\tilde{\boldsymbol{\omega}}]\boldsymbol{\omega}_r) + [\tilde{\boldsymbol{\omega}}_r][I]\boldsymbol{\omega} - \boldsymbol{L}_{\text{ext}}. \tag{22}$$

For the case where electrostatic interactions are not accounted for in the guidance algorithms, the external torque $\boldsymbol{L}_{\text{ext}}$ is assumed to be zero.

5. GUIDANCE

Prior studies into the topic of spacecraft proximity operations guidance under perturbations often focus on optimal control strategies to develop trajectories which minimize risk and fuel consumption [27].

These methods are typically computationally intensive, particularly when applied to systems with significant constraints and complex dynamics, and may require reference trajectories to be computed a priori on the ground, while a controller or neighboring optimal solution follows the trajectory on board the spacecraft [27].

This is often problematic in the case of electrostatic perturbations, which may vary significantly over a several hour rendezvous process as spacecraft move through different local plasma environments, or lighting conditions. This can cause dramatic changes in the relative motion dynamics between the two bodies, necessitating costly recomputation or solutions which may be significantly more fuel-intensive than necessary [28].

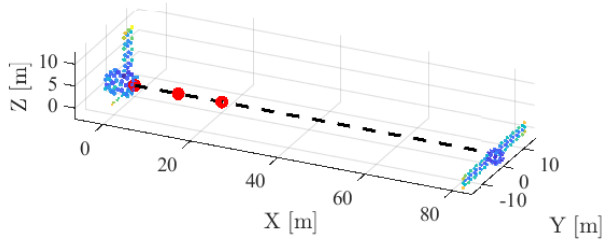

Figure 5. The nominal approach trajectory from the servicer (at $X = 80$ m) to the target (at the origin). Hold points are shown in red.

Instead, the solution introduced here relies on a sampling-based approach, using a reduced-order MSM model to compute position and attitudes which most closely meet a desired torque. The approach trajectory illustrated here defines the servicer position and attitude relative to the target at each time step, providing 6 DOF inputs to the controller.

Several constraints are imposed on the approach trajectory, which is defined with an origin at the docking point as seen in Figure 5. The servicer is required to perform 3 hold maneuvers at 10 meters, 5 meters and 1 meter from the docking point. The first two are set for ten minutes, to allow ground controllers to verify navigation solutions or similar, while the final hold is commanded for 30 minutes to allow for robotic arms to perform grappling maneuvers. Hyperbolic tangent functions are used to smooth the approach trajectory to avoid acceleration singularities. The nominal trajectory with no perturbations is shown in Figure 5, and is shown in the target frame $\mathcal{T}$. For a non-rotating target case, this corresponds to the Hill frame approach.

However, if the target were initially rotating, the servicer will maneuver in the Hill frame to track the reference trajectory in the $\mathcal{T}$ frame. Repulsive electrostatic forces between the target and the servicer result in the target translating relative to the servicer and the servicer having to accelerate to pursue it, these accelerations are very small, on the order of 10^{-7} m/s^2. By comparison, torques result in rotational rates on the order of 0.1/s, which results in translational acceleration of the reference frame relative to the Hill frame, which a servicer at 10 meters distance must then chase with accelerations on the order of 10^{-4} m/s^2 or greater. Electrostatic torques are therefore a much more significant perturbation than electrostatic forces, and minimizing the impact of these torques on an inert target could dramatically reduce the overall control effort required for proximity operation.

Additionally, the final phase of autonomous rendezvous is highly dependent on an accurate navigation solution, typically obtained by a combination of LiDAR and visual or IR cameras. These impose line of sight constraints on the approach trajectory; not only does the servicer need to stay within a constraint cone of the docking point to allow satisfactory navigation sensor visibility, but the attitude of the servicer must also be constrained such that the RPO sensors have a direct line of sight to the docking location. For this work an approach cone with a 25 half angle was chosen, on a similar level to the approach angle observed in publicly available videos of the MEV-1 rendezvous operation. Despite being a relatively tight approach cone, there is significant variation in the magnitude and direction of electrostatic torques acting

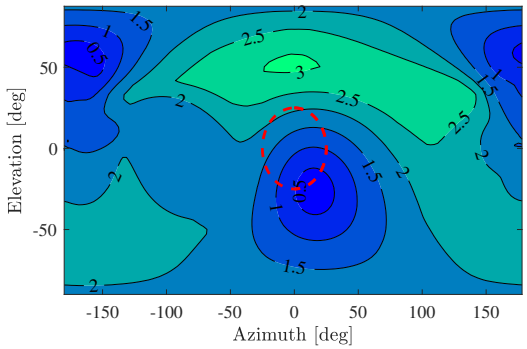

Figure 6. Torque acting on a GOES-R target due to electrostatic interactions at a 10 meter distance as a function of azimuth and elevation. Circled region corresponds to a 25 approach cone.

on the target in this area. Figure 6 illustrates an example of the torques imparted to a GOES-R target with a servicer at 10 meters distance, 10 kV on each spacecraft. Within the 25 approach cone there is a difference of over an order of magnitude between the lowest torque point (< 0.2 mN-m) and the highest (> 2.3 mN-m).

The servicer attitude was then prescribed to orient the sensors towards the docking point, computing the required quaternion between the sensor line of sight vector $\hat{\boldsymbol{s}}$ and the relative $\mathcal{T}$-frame position of the servicer $\boldsymbol{r}_{\text{S/T}}$ as

$$\boldsymbol{c} = \boldsymbol{r}_{\text{S/T}} \times \hat{\boldsymbol{s}} \tag{23}$$

$$\phi = \cos^{-1}\left(\frac{\boldsymbol{r}_{\text{S/T}} \cdot \hat{\boldsymbol{s}}}{|\boldsymbol{r}_{\text{S/T}}||\hat{\boldsymbol{s}}|}\right) \tag{24}$$

$$\boldsymbol{\beta} = [\cos(\phi/2) \quad \boldsymbol{c}\sin(\phi/2)]^T \tag{25}$$

This approach constrains two rotational degrees of freedom for the servicer, but does not constrain the about-boresight rotation.

While only representing one degree of freedom, there can be significant differences in torque exerted on the target at different servicer attitudes. For the example position shown in Figure 8, rotating the servicer about the line of sight axis results in changes in the total torque magnitude of over 60%. In addition, the direction of the torque vector can change by over 70 by varying servicer orientations at a specific position.

The electrostatic torques acting on a target are strongly related to the position of the servicer relative to the target. Figure 6 illustrates the magnitude of electrostatic torques acting on the target as a function of the azimuth and elevation of the servicer with respect to the target. All points are evaluated 10 meters from the nearest surface of the target, and the attitude of the servicer controlled so that it is oriented toward the docking point of the target.

Due the relatively small region admissible under the constraints, a sampling-based strategy can efficiently evaluate the search space. The guidance strategy implemented here evaluates the electrostatic interactions between low-fidelity MSM models (20 sphere) of both spacecraft at 50 points over the 25 approach cone, with a fixed distance to the docking

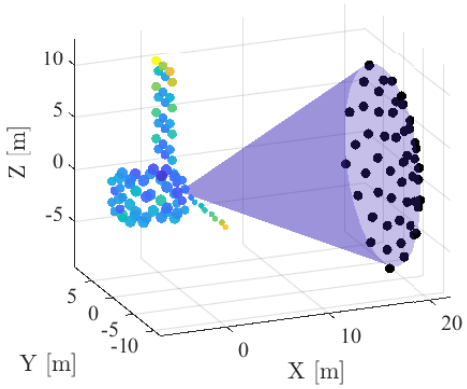

Figure 7. Constraint cone fixed to target docking port, and selected test positions at a fixed distance to the target port.

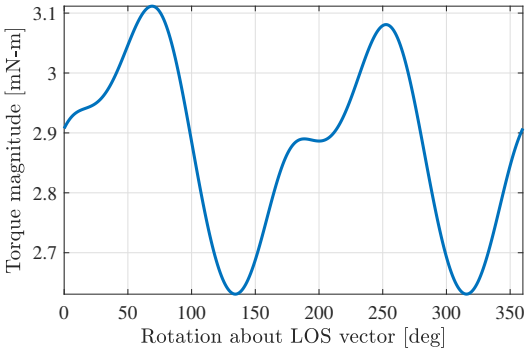

Figure 8. Electrostatic torque imparted to the target as a function of servicer attitude, where the servicer is only rotated about the line of sight (LOS) vector.

location as seen in Figure 7. The position of each point is selected based on a spherical spiral to achieve near evenly spaced points. The number of points to sample is chosen by evaluating the variation in electrostatic torques over the constraint cone, and then setting a density that captures relatively small scale variations in torque with acceptable accuracy. In this case, the sensitivity of torque with respect to angle seen in Figure 6 led to a 50 point sample, which ensures the minimum torque is within 0.1 mN-m of the minimum sampled point. By constraining the distance to the target to be constant, this reduces to a constrained two dimensional (in azimuth and elevation angle) search space, where the L2 norm of the angles must be less than 25.

The electrostatic forces and torques acting between the bodies are a function of the relative position of every sphere on each body, so both the target's attitude and position state need to be prescribed by the guidance algorithm at each timestep. The RPO sensors must maintain a line of sight to the docking point, so the servicer must orient itself accordingly. However, this only constrains two degrees of rotational freedom for the servicer, which is free to rotate about the line of sight. As seen in Figure 8, there can be significant differences in torque as a servicer rotates through the one unconstrained degree of freedom. For this case, the maximum torque is over 20% higher than the minimum, which could have significant implications over a multi-hour proximity operation (a nominal 3 hour approach is used here). Therefore, 50 attitudes are evaluated at each position, to find the combination of position and attitude which come closest to satisfying a desired torque as possible while maintaining a reasonable computational burden.

Evaluating the intercraft forces and torques over 50 attitudes at 50 positions requires less than 1 second using Matlab on a modern laptop computer; significant performance gains could be realized by moving to a language commonly used for flight software development like C. Using a higher fidelity model with four times more spheres per vehicle results in computation times increasing by a factor of $6\times$, with little change in the best position/attitude combination found.

The electrostatic interactions between the servicer and target will evolve over time periods on the order of minutes to tens of minutes, depending on separation distances and closure rates. Therefore, the desired approach vector and attitude combination can be computed relatively infrequently, making this solution well suited to implementation on board a servicing spacecraft. Likewise, the electrostatic potentials on each object are likely to evolve on the order of minutes, so relatively slow updates of the guidance algorithm are well-suited to the dynamics of this problem. However, the MSM formulation tested here is sufficiently fast that it could be implemented on-board a spacecraft with updates on the order of seconds or faster if desired.

For cases where there is no significant difference ($< 1\%$) in electrostatic torque between different orientations, the servicer attitude is chosen to maximize the distance between the closest points on the two spacecraft in an effort to minimize the probability of a collision between the craft.

Additionally, there are cases where exerting a specific electrostatic torque on the target may be desirable. These could cover scenarios involving rendezvous with a tumbling target, when electrostatic forces can help reduce the rotational rate of the target prior to grappling, or cases where a cooperative client transitions into a free-drift mode prior to docking and perturbing effects like SRP could be negated by electrostatic interactions.

6. Simulation Results

A rendezvous scenario is simulated with a notional GEO spacecraft and servicer. The target spacecraft is based on the NOAA GOES-R weather satellite, which has significant amounts of data published in existing literature documenting dimensions and masses; CAD models are then developed to estimate the center of mass location and inertia properties. These properties are then taken to be known exactly in the controller and dynamics propagation.

SRP was added as an unmodeled disturbance for the target body, using the non-shadowing model discussed previously. For the GOES-R target, the single asymmetric solar array leads to average SRP induced torques of approximately 0.5 mN-m across all orientations. For comparison, electrostatic torques at 10 meters exceed this level when just 1900V are applied to each spacecraft.

The guidance method proved to significantly reduce the total rotational rates imparted to the target prior to docking, which can result in improved docking accuracy, reduced navigation uncertainty and more predictable lighting conditions. These improvements occur despite not accounting for significant SRP torques in the model. Steady lighting conditions are

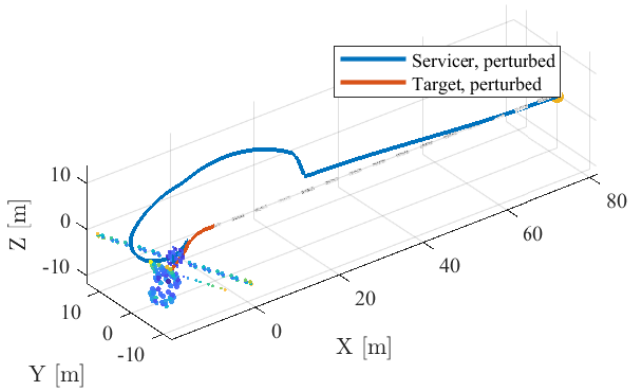

Figure 9. Rendezvous trajectory perturbed by 10kV electrostatic potential on each spacecraft, with no guidance accounting for electrostatic interactions.

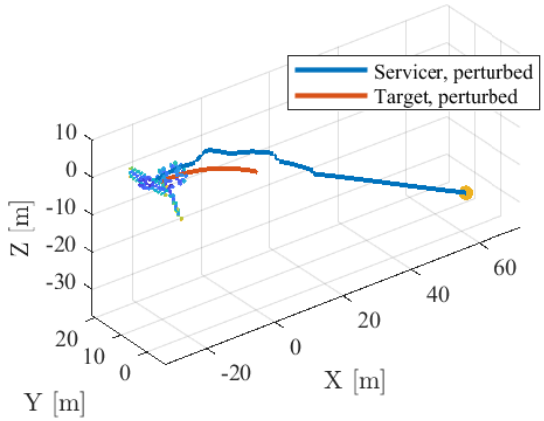

Figure 10. Rendezvous trajectory perturbed by 10kV electrostatic potential on each spacecraft, with guidance accounting for electrostatic interactions to reduce the total torque imparted to the target.

particularly important in improving optical navigation accuracy during the final meters of rendezvous, when small errors could result in undesired contact between the spacecraft.

Figure 9 illustrates a straight line rendezvous perturbed by electrostatic interactions, using a guidance policy that does not account for those electrostatic perturbations. The dashed line illustrates the trajectory unperturbed by electrostatics. Qualitatively, the approach shown in Figure 10 experiences far less perturbation from the nominal, straight line trajectory shown in Figure 9. These simulations are performed with 80 sphere models for the target and 92 spheres for the servicer, and 10 kV potentials on each. This is a severe charging event only relatively infrequently at GEO, but is reasonable to anticipate in a spacecraft lifetime [2]. This scenario therefore offers a plausible instance of significant electrostatic perturbations due to space weather interactions.

Selecting an approach angle to minimize the electrostatic forces acting on the target during rendezvous results in a greater than 60% decrease in control effort required for rendezvous, and decreases in target rotational rate of over 50%, from $0.025/s$ to less than $0.01/s$.

For this analysis both spacecraft are assumed to be at fixed potentials, with electrostatic potentials constant over the entire spacecraft surface. This is in adherence with modern guidelines for spacecraft design, which recommend that all surfaces be continuously conducting and commonly grounded to the spacecraft frame to mitigate arcing hazards. However, this is not an accurate assumption in all cases; older spacecraft were frequently nonconducting, which can result in different components on the structure having potential differences of hundreds or even thousands of volts due to varying material properties and solar photon exposure [18], [6]. Inclusion of differential charging effects and the assessment of their impact in proximity operations is an area for future work, and could be augmented by the approach presented in Reference [29] for incorporating non-conductive structures into an MSM framework.

Given the attitude, position and approach angle constraints imposed on the servicer, only a limited subset of potential locations are admissible. While the sampling-based method used here may only find a sub optimal local minimum of the electrostatic torque, it is likely to be within ~ 0.1 mN-m of an absolute minimum torque. This limits the improvements in performance that can be realized through the use of more computationally intensive optimal control strategies. While it is expected that the servicer should be able to determine its own attitude with high precision, uncertainty in target relative pose estimation can drive significant mis-calculation of the electrostatic torques between the craft. Taking the gradient of the data shown in Figure 6 allows the sensitivity of torque to the attitude of the target to be determined. Some regions exhibit sensitivities of up to 0.04 mN-m/degree, so just a few degrees of error in target attitude estimates can result in fairly significant errors in computed electrostatic torque.

7. Conclusions

While electrostatic perturbations can significantly impact proximity operations dynamics, it is possible to use new methods to remotely sense the potential on an object in tandem with rapid techniques for evaluating the resultant inter-craft forces and torques to mitigate these concerns. The impact of electrostatic interactions can be reduced substantially, without imposing unreasonable burdens on operational constraints or computational resources.

For targets that are poorly characterized or otherwise difficult to obtain accurate pose estimates for, it may be advantageous to optimize for both torque and pose estimation sensitivity. This could allow a relatively low, but not minimal, torque to be found, but with less impact from potential errors in target pose estimates. Additional work is underway to extend the applicability of this method to reducing the final rotational rate of a target with an initial tumble rate. While this method provides a rapid estimate of a near-optimal position and attitude for the approaching servicer given operationally imposed constraints, future work will further compare the results of this method to a model predictive control-based solution.

References

[1] K. Wilson and H. Schaub, "Impact of electrostatic perturbations on proximity operations in high earth orbits," in *AAS/AIAA Astrodynamics Specialist Conference*, Lake Tahoe, CA, Aug. 9–13 2020.

[2] R. Olsen, "The record charging events of ats-6," *Journal of Spacecraft and Rockets*, vol. 24, 1987. [Online]. Available: https://calhoun.nps.edu/handle/10945/36749

[3] K. T. Wilson, M. Bengtson, and H. Schaub, "Hybrid method of remote sensing of electrostatic potential for proximity operations," in *IEEE Aerospace Engineering Conference*, Big Sky, MO, March 7–14 2020.

[4] J. A. Hughes and H. Schaub, "Heterogeneous surface multisphere models using method of moments foundations," *Journal of Spacecraft and Rockets*, vol. 56, no. 4, pp. 1259–1266, 2019.

[5] J.-C. Matéo-Vélez, A. Sicard, D. Payan, N. Ganushkina, N. P. Meredith, and I. Sillanpäa, "Spacecraft surface charging induced by severe environments at geosynchronous orbit," *Space Weather*, vol. 16, no. 1, pp. 89–106, 2018.

[6] R. C. Olsen, C. E. McIlwain, and E. C. Whipple Jr., "Observations of differential charging effects on ats 6," *Journal of Geophysical Research: Space Physics*, vol. 86, no. A8, pp. 6809–6819, 1981.

[7] H. Koons, J. Mazur, A. Lopatin, D. Pitchford, A. Bogorad, and R. Herschitz, "Spatial and temporal correlation of spacecraft surface charging in geosynchronous orbit," *Journal of Spacecraft and Rockets*, vol. 43, no. 1, 2006.

[8] M. Cho, S. Kawakita, M. Nakamura, M. Takahashi, T. Sato, and Y. Nozaki, "Number of arcs estimated on solar array of a geostationary satellite," *Journal of Spacecraft and Rockets*, vol. 42, no. 4, pp. 740–748, 2005.

[9] S. T. Lai, *Fundamentals of Spacecraft Charging: Spacecraft Interactions with Space Plasmas*. Princeton University Press, 2011.

[10] W. H. Clohessy and R. S. Wiltshire, "Terminal guidance system for satellite rendezvous," *Journal of the Aerospace Sciences*, vol. 27, no. 9, pp. 653–658, Sept. 1960.

[11] H. Schaub and J. L. Junkins, *Analytical Mechanics of Space Systems*, 4th ed. Reston, VA: AIAA Education Series, October 2019.

[12] J. E. Borovsky and M. H. Denton, "Magnetic field at geosynchronous orbit during high-speed stream-driven storms: Connections to the solar wind, the plasma sheet, and the outer electron radiation belt," *Journal of Geophysical Research: Space Physics*, vol. 115, no. A8, 2010.

[13] W. Baumjohann and R. A. Treumann, *Basic Space Plasma Physics*. PUBLISHED BY IMPERIAL COLLEGE PRESS AND DISTRIBUTED BY WORLD SCIENTIFIC PUBLISHING CO., 1996.

[14] S. Spiridonova and R. Kahle, "Relative orbit dynamics in near-geostationary orbit," in *International Symposium on Space Flight Dynamics* , Munich, Germany, Oct. 19–23 2015.

[15] M. List, S. Bremer, Benny, and H. Selig, "Modelling of solar radiation pressure effects: Parameter analysis for the microscope mission," *International Journal of Aerospace Engineering*, 2015.

[16] D. Stevenson and H. Schaub, "Multi sphere modeling for electrostatic forces on three-dimensional spacecraft shapes," in *AAS/AIAA Spaceflight Mechanics Meeting*, Charleston, South Carolina, Jan. 29 – Feb. 2 2012.

[17] J. Maxwell, K. Wilson, J. Hughes, and H. Schaub, "Multisphere method for flexible conducting space objects: Modeling and experiments," *AIAA Journal of Spacecraft and Rockets*, vol. 57, no. 2, pp. 225–234, 2020.

[18] L. K. Sarno-Smith, B. A. Larsen, R. M. Skoug, M. W. Liemohn, A. Breneman, J. R. Wygant, and M. F. Thomsen, "Spacecraft surface charging within geosynchronous orbit observed by the van allen probes," *Space Weather*, vol. 14, no. 2, pp. 151–164, 2016.

[19] K. Wilson, M. Bengtson, and H. Schaub, "X-ray spectroscopic determination of electrostatic potential and material composition for spacecraft: Experimental results," *Space Weather*, vol. 18, no. 4, pp. 1–10, April 2020.

[20] K. Wilson and H. Schaub, "Environmental x-ray considerations for bremsstrahlung-based surface potential determination," in *AIAA SciTech*, Orlando, Florida, Jan. 6–10 2020.

[21] M. Bengtson, J. Hughes, and H. Schaub, "Prospects and challenges for touchless sensing of spacecraft electrostatic potential using electrons," *IEEE Transactions on Plasma Science*, 2019.

[22] D. M. Perfetto, R. Opromolla, M. Grassi, and C. Schmitt, "Lidar-based model reconstruction for spacecraft pose determination," in *2019 IEEE 5th International Workshop on Metrology for AeroSpace (MetroAeroSpace)*, 2019, pp. 1–6.

[23] R. Opromolla, G. Fasano, G. Rufino, and M. Grassi, "Uncooperative pose estimation with a lidar-based system," *Acta Astronautica*, vol. 110, pp. 287 – 297, 2015.

[24] D. Ivanov, M. Ovchinnikov, and M. Sakovich, "Relative pose and inertia determination of unknown satellite using monocular vision," *International Journal of Aerospace Engineering*, 09 2018.

[25] E. Hogan and H. Schaub, "Relative motion control for two-spacecraft electrostatic orbit corrections," *AIAA Journal of Guidance, Control, and Dynamics*, vol. 36, no. 1, pp. 240–249, Jan. – Feb. 2013.

[26] T. Marshall and M. Fletcher, "Meeting high-qualitiy rwa commercial demand through innovative design," in *Space Mechanisms and Tribology, Proceedings of the 8th European Symposium*, 1999.

[27] Y. Luo, J. Zhang, and G. Tang, "Survey of orbital dynamics and control of space rendezvous," *Chinese Journal of Aeronautics*, vol. 27, no. 1, pp. 1 – 11, 2014.

[28] J. E. Mazur, J. F. Fennell, J. L. Roeder, P. T. O'Brien, T. B. Guild, and J. J. Likar, "The timescale of surface-charging events," *IEEE Transactions on Plasma Science*, vol. 40, no. 2, pp. 237–245, 2012.

[29] J. Hughes and H. Schaub, "Guidance, navigation and control advances in electrostatic attitude control on passive geo objects," in *9th International Workshop on Satellite Constellations and Formation Flying*, Boulder, CO, June 19–21 2017, paper No. IWSCFF 17-16.

BIOGRAPHY

Kieran Wilson *is a graduate research assistant at the University of Colorado Boulder in the Aerospace Engineering Sciences Department. He received B.S. degrees in Aerospace Engineering and Mechanical engineering from the University of Florida in Gainesville, FL, and MS in Aerospace Engineering from the University of Colorado Boulder. Kieran's research interests include charged astrodynamics, proximity operations and remote sensing of spacecraft potentials.*

Hanspeter Schaub *Dr. Schaub is a professor in the Aerospace Engineering Sciences department and the Glenn L. Murphy Chair in Engineering at the University of Colorado. He has over 20 years of research experience, of which 4 years are at Sandia National Laboratories. His research interests are in nonlinear dynamics and control, astrodynamics, relative motion dynamics, as well as relative motion sensing. In the last decade he has developed the emerging field of charged astrodynamics. Dr. Schaub has been the ADCS lead in the CICERO mission and the ADCS algorithm lead on a Mars Mission. He is an AAS and AIAA Fellow, and has won the AIAA/ASEE Atwood Educator award, as well as the AIAA Mechanics and Control of Flight award. He currently serves as the Editor-In-Chief for the AIAA Journal of Spacecraft and Rockets.*